Thermal frequency noise in Dynamic Scanning Force Microscopy

J. Colchero, M. Cuenca, J.F. González Martínez, J.
Abad, B. Pérez García, E. Palacios-Lidón and J. Abellán
Facultad de Quimica, Departamento de Física,
Universidad de Murcia, E-30100 Murcia.

Abstract

Thermal fluctuation of the cantilever position sets a fundamental limit for the precision of any Scanning Force Microscope. In the present work we analyse how these fluctuations limit the determination of the resonance frequency of the tip-sample system. The basic principles of frequency detection in Dynamic Scanning Force Microscopy are revised and the precise response of a typical frequency detection unit to thermal fluctuation of the cantilever is analysed in detail. A general relation for thermal frequency noise is found as a function of measurement bandwidth and cantilever oscillation. For large oscillation amplitude and low bandwidth, this relation converges to the result known from the literature, while for low oscillation amplitude and large bandwidth we find that the thermal frequency noise is equal to the width of the resonance curve and therefore stays finite, contrary to what is predicted by the relation known so far. The results presented in this work fundamentally determine the ultimate limits of Dynamic Scanning Force Microscopy.

I. INTRODUCTION

Since its invention Scanning Force Microscopy (SFM)[1] has become an extremely powerful tool for a huge variety of nanoscale investigations. With respect to resolution and sensitivity, Dynamic Scanning Force Microscopy (DSFM)[2] seems to be the most promising technique. Even though (true) atomic resolution was first achieved with contact mode in liquid environment[3], now atomic resolution studies are generally performed with DSFM working in UHV environment[4–6]. Recently even sub-atomic resolution has been reported using DSFM [7]. In spite of the impressing advances of SFM and DSFM we believe that the ultimate limit of these techniques is still an open issue. For most applications, the temperature at which quantum limits become relevant, $T_Q = \hbar\omega_0/k \simeq 1\mu K$, is well below typical temperature ranges used in SFM. Correspondingly, either thermal vibration of the cantilever[8–10], or fundamental limits of the detection technique used[11–13] - related to shot noise of the "detection particles" - determine the resolution in SFM and DSFM. In most practical applications, the fundamental limit of SFM and DSFM is set by thermal noise. Thermal noise in an SFM set up is the consequence of the equipartition theorem, which relates the mean energy of the cantilever with the thermal energy kT,

$$\frac{1}{2}c\ a_{th}^2 = \frac{1}{2}kT \tag{1}$$

where a_{th}^2 is the (mean square) displacement of the cantilever induced by thermal fluctuation, and c is its force constant. For high resolution distance measurements stiff cantilevers[14, 15] should be used ($\delta z = \sqrt{kT/c}$, with δz fluctuation of tip-sample distance), while for high resolution force measurements soft cantilevers[16] are needed ($\delta F_{th} = c \cdot a_{th} = \sqrt{c\ kT}$). Although the mean displacement and the mean force fluctuation of the cantilever are important quantities, in many applications they do not directly determine resolution, either because appropriate filtering significantly reduces the measured noise, or because the SFM technique used -as for example DSFM- is not directly limited by the displacement or the force.

In typical DSFM applications the cantilever is excited at or near its natural frequency and the variation of its resonant properties -oscillation amplitude, resonance frequency or quality factor - are recorded. For imaging applications in liquids or air usually the oscillation amplitude is used as control parameter that defines constant tip-sample distance and the frequency shift is measured as secondary channel. In Ultra High Vaccum (UHV) applications

DSFM operation is the other way, the frequency shift is the control parameter for tip-sample distance and the oscillation amplitude -dissipation energy- is measured as secondary channel. At the moment DSFM is the most sensitive SFM technique to measure tip-sample interaction, which is detected as a shift of the resonance frequency. Therefore, with regard to the ultimate limits of SFM a key issue -to be discussed in the present work- is to understand in detail the effect of thermal fluctuations on DSFM detection schemes and in particular on frequency detection. At present, the thermal noise density of a frequency measurement is assumed to be[17, 18, 20]

$$\frac{\Delta\nu_{th}}{\nu_0} = \sqrt{\frac{kT}{\pi\ c\ a^2\ \nu_0\ Q}}\sqrt{bw} \tag{2}$$

with Q the quality factor, ν_0 the resonance frequency, a the (root mean square) oscillation amplitude and bw the bandwidth of the measurement. Note that this relation diverges for small oscillation amplitude and is proportional to the square root of the measurement bandwidth.

In the present work we will revise in detail how thermal fluctuation limits the measurement of frequency shift. We find that neither for large bandwidth measurements nor for low oscillation amplitude relation 2 is correct. We present a general relation valid for all ranges of amplitude and bandwidth that agrees with relation 2 in the low bandwidth and large amplitude range. Finally, we present experimental data that unambiguously proves the validity of the general relation obtained in this work.

II. FREQUENCY DETECTION IN DYNAMIC SCANNING FORCE MICROSCOPY

A. Mathematical modelling of a Dynamic Scanning Force Microscopy detection electronics

A thorough discussion of frequency detection and DSFM is out of the scope of the present work (see the excellent original works[17, 18] or recent reviews by Garcia and Perez[19] and Giessibl[20]), nevertheless we think it is important to revise some of its basic principles. The focus of this revision is rather on a comprehensive physical explanation of the technique than on a profound analysis of the underlying physiscs and statistical mechanics (see[18]) or the electronic details of its implementation(see [18, 21]).

An externally driven SFM cantilever -usually driven by inertial forces- is a textbook example of a harmonic oscillator. In many aspects SFM and modern gravitational wave detectors are governed by the same basic principles (see, for example, [22]). As described in detail in appendix A, the dynamic properties of such a system are described by the quality factor Q, by a driving amplitude a_0 and by its natural angular frequency $\omega_0 = 2\pi\nu_0 = \sqrt{c/m_{eff}}$, with ν_0 natural frequency and m_{eff} effective mass of the cantilever[23]. In the steady state regime, the response of the system to a harmonic excitation $a_0\omega_0^2\cos(2\pi\nu t)$ can be described by a (complex) amplitude $A(\nu)$, or by two components $X(\nu)$ and $Y(\nu)$, the in-phase and out of phase components of the oscillation, corresponding to the real and complex parts of the complex amplitude $A(\nu)$. The time response of the system is then $a(t) = X(\nu)\cos(2\pi\nu t) + Y(\nu)\sin(2\pi\nu t) = |A(\nu)|\cos(2\pi\nu t + \varphi(\nu))$ where $\varphi(\nu)$ is the phase between the driving force and the response. At its natural frequency ν_0 the phase is $-\pi/2$, the (complex) oscillation amplitude is $A(\nu_0) = -iY(\nu_0) = -ia_0Q$ and the in-phase component $X(\nu_0)$ vanishes.

Figure 1 shows a schematic set-up of the main components used in a DSFM detection electronics. The multiplication stages together with the filters essentially calculate the two components $X(\nu)$ and $Y(\nu)$ -relations 19 and 20 in appendix A- from the measured oscillation of the cantilever $a(t)$. When enabled, the PI-controller of the DSFM detection electronics adjusts the driving frequency ν of the excitation signal in order to have $X(\nu) = 0$. In this way, the system is locked to the natural frequency of the cantilever, tracks this frequency if it varies due to tip-sample interaction and generates an output proportional to the shift of the resonance frequency. In addition to the main DSFM components figure 1 shows the signals (in the frequency domain) along the different points in the DSFM detection path. A key component of any DSFM detection unit is the voltage (VCO) or numerically (NCO) controlled oscillator that generates the excitation and reference signals for the lock-in detection scheme. In most applications this oscillator drives the piezo that induces motion of the cantilever. The corresponding deflection $a(t)$ is analyzed by multiplication with two reference signals in quadrature. We will first assume the most general case where the frequency ν of the cantilever motion and that of the reference oscillator are different. Then, multiplication of the deflection signal $a(t) = a_0\cos(2\pi\nu t + \varphi(\nu))$ with the reference signal $a_{ref}(t) = \cos(2\pi\nu_{ref}t)$ results in two quadrature signals $x_q(t) = a(t)\cos(2\pi\nu_{ref}t)$ and $y_q(t) = a(t)\sin(2\pi\nu_{ref}t)$ with frequency components at $\nu_\Delta = \nu - \nu_{ref}$, and $\nu_\Sigma = \nu + \nu_{ref}$. As

shown in appendix A, $x_q(t)$ and $y_q(t)$ can be obtained from $X(\nu)$ and $Y(\nu)$ by multiplication with $(\mathbf{M}_\Delta(t) + \mathbf{M}_\Sigma(t))$, where $\mathbf{M}_\Delta(t)$ is a rotation matrix generating a clockwise rotation with frequency ν_Δ, and $\mathbf{M}_\Sigma(t)$ is a rotation matrix generating a counter-clockwise rotation with frequency ν_Σ. In the frequency domain the signal $a(t)$ is thus splitted and shifted to the sum and to the difference frequency (see figure 1). After the multiplication stages the two quadrature signals $x_q(t)$ and $y_q(t)$ are low-pass filtered over a timespan proportional to the time constant τ of the filter. The precise time domain signals are determined in appendix A. Again, two matrices $\mathbf{M}\tau_\Delta(t)$ and $\mathbf{M}\tau_\Sigma(t)$ can be defined (relations 25 and 26 in appendix A), corresponding to a clockwise and counter-clockwise rotation with the frequencies ν_Δ and ν_Σ. As compared to the first matrices, these "filtered" matrices have delay angles $\varphi_\Delta(\tau)$ and $\varphi_\Sigma(\tau)$ as well as multiplicative factors $1/(1+4\pi^2\tau^2\nu_\Delta^2)$ and $1/(1+4\pi^2\tau^2\nu_\Sigma^2)$.

Usually, in DSFM the signal entering the DSFM detection unit is at the natural frequency ν_0, and the reference is at the same frequency $\nu_{ref} = \nu_0$. Then multiplication of the input signal with the reference signals will result in spectra around $\nu = 0$ and $\nu = 2\nu_0$. In this case $\mathbf{M}\tau_\Delta(t) = \mathbf{Id}/2$, with $\mathbf{Id}$ the identity matrix, and we find, using relations 25 and 26 (see Appendix A):

$$\langle x_q(t)\rangle_\tau = \frac{X(\nu)}{2} + \frac{X(\nu)(\cos(2\omega_0 t) - 2\omega_0\tau\sin(2\omega_0 t))}{2\,(1+4\omega_0^2\tau^2)} + \frac{Y(\nu)(\sin(2\omega_0 t) + 2\omega_0\tau\cos(2\omega_0 t))}{2\,(1+4\omega_0^2\tau^2)} \tag{3}$$

$$\langle y_q(t)\rangle_\tau = \frac{Y(\nu)}{2} + \frac{X(\nu)(\sin(2\omega_0 t) + 2\omega_0\tau\cos(2\omega_0 t))}{2\,(1+4\omega_0^2\tau^2)} + \frac{Y(\nu)(-\cos(2\omega_0 t) + 2\omega_0\tau\cos(2\omega_0 t))}{2\,(1+4\omega_0^2\tau^2)} \tag{4}$$

These signals can be conveniently represented in the frequency domain (see fig.1), where the first peak at $\nu = 0$ is one-sided (since no negative frequency exists) and the second at $\nu = 2\nu_0$ is two-sided. In typical DSFM applications the filter is usually set so that $\nu_0 >> 1/\tau$, then it blocks the $2\nu_0$ component and passes the signals from DC to $\nu_{fil} \approx 1/\tau$. The value of τ determines the speed and the "cleanness" of the signals. Large time constants (small bandwidth) results in clean but slow response, while, conversely, small-time constants will result in "unclean" signals – in particular with significant $2\nu_0$ component - but with fast response. In our system we have found that time constants of $3/\nu_0$ to $10/\nu_0$ give the optimum compromise between speed and "cleanness".

In the frequency domain, the Fourier transforms of the signals $x_q(t)$ and $y_q(t)$ are simply multiplied by the frequency-dependent gain of the filter. Depending on the time constant of the filter, the total amount of signal may be decreased. The calculation of the total signal $\Delta u_{bw}(\nu_c)$ measured around a frequency ν_c within a certain bandwidth bw is performed most conveniently in frequency domain:

$$\Delta u_{bw}(\nu_c) = \sqrt{\int_{\nu_c - bw/2}^{\nu_c + bw/2} d\nu \; v^2(\nu)} \tag{5}$$

where $v(\nu)$ is the (spectral) signal density (unit: $V/\sqrt{Hz}$) and $bw = 1/\tau$ the effective bandwidth of the filter. The signal densities corresponding to $\langle x(t)\rangle_\tau$ and $\langle y(t)\rangle_\tau$ in the frequency domain are $X_q(\nu)G_{fil}(\nu)$ and $Y_q(\nu)G_{fil}(\nu)$, respectively, being $X_q(\nu)$ and $Y_q(\nu)$ the Fourier transforms of the quadrature signals $x_q(t)$ and $y_q(t)$, and $G_{fil}(\nu) = 1/(1+i2\pi\nu\tau)$ the (complex) gain of the filter (see figure 1).

B. Phase Locked Loop operation

If the Q factor is low -as in air and in liquids- the signals $\langle x(t)\rangle_\tau$ and $\langle y(t)\rangle_\tau$ can be directly used for DSFM. In fact, for low Q factors and low tip-sample interaction the frequency shift $\Delta\nu_{int}$ induced by tip-sample interaction is smaller than the width of the resonance ($\Delta\nu_{int} < \nu_0/Q$). Assuming the validity of the harmonic approximation for the dynamics of the cantilever, the signal $\langle x(t)\rangle_\tau$ is then proportional to the frequency shift, and the signal $\langle y(t)\rangle_\tau$ is proportional to the oscillation amplitude, which in air and liquids is generally used as control parameter. For high Q factors, however, the width of the resonance is smaller than the frequency shifts induced by tip-sample interaction. Moreover, high Q-factors imply that the oscillation amplitude needs a long settling time (of the order of Q/ν_0) to reach its steady state value[17]. In this case it is necessary to track the resonance frequency using Phase Locked Loop techniques[17, 18, 21]. This is implemented with a PI-controller that essentially adjusts the frequency of the voltage or numerically controlled oscillator (VCO or NCO, see fig. 1) so that the $\langle x(t)\rangle_\tau$ component vanishes; the phase of the oscillation is then kept at $-\pi/2$ and the system is always at resonance. The output of the PI-controller is then directly proportional to the frequency shift, and this is the signal used in typical DSFM applications. The PI-controller represents, from an electronic point of view, a filter with a well defined bandwidth and gain. The time constant of the filters following the

multiplication stages and the bandwidth and gain of the PI-controller have to be chosen so that the overall closed loop system is stable[18]. Since the precise set up of the PI-controller does not modify the essential physics to be discussed here we will assume - to simplify the discussion - an ideal controller that instantaneously transmits variations of $\langle x(t)\rangle_\tau$ to the VCO. The time response of the overall system is then determined by the time constant of the filters after the multiplication stage, which induce a delay of order τ.

III. THERMAL FLUCTUATION OF THE CANTILEVER POSITION

In addition to the "coherent" signal $a_{ex}(t)$ induced by the external excitation of the cantilever, in the present context also the "incoherent" contribution due to thermal noise, $a_{th}(t)$, is important[18]. The total motion of the cantilever is thus $a(t) = a_{ex}(t) + a_{th}(t)$. When this motion is transduced into an electrical signal, the position detector will add some instrumental noise $n(t)$, the total signal entering the DSFM detection unit is then $u_{DSFM}(t) = e\ (a_{ex}(t) + a_{th}(t)) + n(t)$, where e is a constant that describes the sensitivity (unit:V/nm) of the photodetector electronics. The key question is now: how does this signal pass the DSFM detection unit and what is the final noise of the frequency output?

The Equipartition Theorem discussed above (relation 1) relates the total thermal displacement to the force constant of the cantilever and the temperature of the system. However, since the DSFM detection system performs non-trivial processing of the input signal, the precise spectrum of the thermal noise has to be taken into account in order to calculate the noise of the frequency output and thus the precise limit of DSFM. A detailed discussion of thermal noise in SFM set-ups is out of the scope of the present work (see, for example[9, 10, 18, 24]). In a simple picture, the noise density of the cantilever motion can be obtained by observing that the Equipartition Theorem (equation 1) relates the mean energy of the cantilever with the thermal energy kT. Assuming that the effective thermal noise "force" driving the cantilever has a constant spectral density α_{th} (unit: $nm/\sqrt{Hz}$), this density and the mechanical gain $G(\nu)$ of the cantilever (relation 18, Appendix A) determine the spectral response of the of the cantilever: $a_{th}(\nu) = \alpha_{th}\ G(\nu)$. The Equipartition Theorem (relation 1) then implies:

$$\frac{1}{2}kT = \int_0^\infty d\nu\ \frac{c}{2}a_{th}^2(\nu) = \frac{c}{2}\ \alpha_{th}^2\ \nu_0 \int_0^\infty \frac{d\nu}{\nu_0}\ \frac{1}{(1-(\nu/\nu_0)^2)^2 + ((\nu/\nu_0)/Q)^2}$$

The second integral gives $Q\ \pi/2$, therefore the thermal noise density α_{th} is

$$\alpha_{th} = \sqrt{\frac{2\ kT}{\pi\ c\ \nu_0\ Q}} \tag{6}$$

The thermal noise density defines the coupling of the thermal bath into the SFM system. It depends on the quality factor and thus on the dissipation properties of the system. As the quality factor increases, thermal fluctuations induce less "thermal force" on the system, that is, coupling of the thermal bath and the tip-sample system becomes weaker.

The thermal fluctuation of the cantilever position measured experimentally with a DSFM detection unit is calculated from the noise density in analogy to relation 5:

$$\Delta a_{th}\left(\nu_c, bw\right) = \alpha_{th}\sqrt{\int_{\nu_c - bw/2}^{\nu_c + bw/2} d\nu\ \left|G(\nu)\right|^2} \tag{7}$$

For low frequencies, that is, for frequencies well below the resonance frequency $G\left(\nu\right) = \alpha_{th}$ and the total thermal fluctuation within a bandwidth bw is

$$\Delta a_{th}\left(\nu_c, bw\right) \simeq \alpha_{th}\sqrt{bw} \tag{8}$$

At the resonance frequency $G\left(\nu\right) = \alpha_{th}Q$ and the total thermal fluctuation is

$$\Delta a_{th}\left(\nu_0, bw\right) \simeq \alpha_{th}Q\sqrt{bw} = \sqrt{\frac{2\ kT\ Q}{\pi\ c\ \nu_0}}\sqrt{bw} \tag{9}$$

as is well known from the literature [17, 18, 20]. While relation 8 is correct for static SFM applications, relation 9 requires the condition that the measurement bandwidth is smaller than the width of the resonance curve: $bw \simeq 1/\tau \ll \nu_0/Q$. We note that in general this assumption may not be correct. In fact, for typical imaging applications (scan speed of 1 second/line, 250 points/line) a minimum bandwidth of 250Hz is required, which implies $Q \ll 4000$ for typical cantilevers ($\nu_0 \simeq 100$ kHz) in order to fulfill the "small bandwidth" approximation. However, in UHV much higher Q values have been reported[25]. Relation 9 overestimates the thermal noise for large bandwidth. In fact, for $bw > (\pi/2)(\nu_0/Q)$ the total thermal noise according to relation 9 would be larger than $\sqrt{kT/c}$, which is non-physical since it is in contradiction with the Equipartition Theorem (rel. 1). As discussed below, for a sufficiently large bandwidth the total thermal noise is $\Delta a_{th} = \sqrt{kT/c}$ and is independent of the measuring bandwidth.

A simple illustrative approximation for the spectral noise density of the tip-sample system is

$$\alpha_{appr}(\nu) = \left\{ \begin{array}{ll} \sqrt{\frac{Q}{Q+1}}\alpha_{th} & \text{for } 0 \leq \nu < \nu_0\,(1-\delta) \text{ and } \nu_0\,(1+\delta) < \nu < \nu_0\,(1+2\delta) \\ \sqrt{\frac{Q}{Q+1}}Q\ \alpha_{th} & \text{for } \nu_0\,(1-\delta) < \nu < \nu_0\,(1+\delta) \\ 0 & \text{for } \nu \geq \nu_0\,(1+2\delta) \end{array} \right\}$$

with $\delta = \pi/(4\ Q)$. This approximation shown in figure 2 satisfies, as the correct noise density, the relations $\alpha_{appr}(\nu_0) = Q\ \alpha_{appr}(0)$, width of the peak of the order ν_0/Q, total noise $\Delta a = \left(\int d\nu\ \alpha^2_{appr}(\nu)\right)^{1/2} = \sqrt{kT/c}$ and, for large Q, $\alpha(0) = \alpha_{th}$. The relation of noise in the "peak", to that in the "flat" part is $\Delta a_{peak}/\Delta a_{flat} = Q$. For high Q factors most of the noise is in the resonance peak of the curve, and $\Delta a_{peak} \approx \Delta a_{total} = \sqrt{kT/c}$. Therefore DSFM does not reduce but rather increase the total thermal noise as compared to static SFM. However, the signal to noise ratio is not modified: at low frequencies (static SFM) a driving force f_0 will induce the motion $a_0 = f_0/c$, and the signal to noise ratio is $a_0/(\alpha_{th}\sqrt{bw})$, while if this force is applied at resonance it will induce a response Qa_0 and, for sufficiently small bandwidth, the thermal noise is $Q\alpha_{th}\sqrt{bw}$. Noise and signal are therefore amplified equally. Correspondingly, DSFM increases sensitivity by a factor of Q as compared to static SFM, but the (theoretical) signal to noise ratio is unchanged. Finally, we note that in normal applications the thermal fluctuations of the x and y component are uncorrelated, and that both should have the same amount of fluctuation (see, however, [26]). Then, since $\langle a^2_{th}(t)\rangle_\tau = \left\langle |x_{th}(t) + i\ y_{th}(t)|^2 \right\rangle_\tau = \langle x^2_{th}(t) + y^2_{th}(t)\rangle_\tau = \langle x^2_{th}(t)\rangle_\tau + \langle y^2_{th}(t)\rangle_\tau$, it follows that $\langle x^2_{th}(t)\rangle_\tau = \langle y^2_{th}(t)\rangle_\tau = \langle a^2_{th}(t)\rangle_\tau /2$, therefore

$$\Delta x_{th}\,(\nu_c, bw) = \Delta y_{th}\,(\nu_c, bw) = \Delta a_{th}\,(\nu_c, bw)\,/\sqrt{2} \tag{10}$$

and for the total thermal fluctuation of the x and y components: $\Delta x_{th} = \Delta y_{th} = a_{th}/\sqrt{2} = \sqrt{kT/\,(2c)}$.

IV. FREQUENCY RESPONSE OF DSFM DETECTION SCHEMES TO THERMAL FLUCTUATIONS

To calculate the frequency noise, the relation

$$\Delta\nu_{th} = \left|\frac{\partial\nu}{\partial\varphi}\right| \Delta\varphi_{th} = \left|\left(\frac{\partial\varphi}{\partial\nu}\right)^{-1}\right| \Delta\varphi_{th} \tag{11}$$

will be used. With $\partial\varphi(\nu_0)/\partial\nu = -2Q/\nu_0$ (see relation 21, appendix A) the only unknown quantity is the phase noise $\Delta\varphi_{th}$. The phase, as defined by relation (21) is $\varphi(t) = -\pi/2 + \tan^{-1}(x(t)/y(t))$. We will assume that DSFM is operated in the Phase Looked Loop mode and is thus always at resonance; then $\langle x(t)\rangle_\tau = \langle a_{th}(t)/\sqrt{2}\rangle_\tau = 0$ and $\langle y(t)\rangle_\tau = \langle Qa_0 + a_{th}(t)/\sqrt{2}\rangle_\tau = a_{os}$, with $a_{os} = Qa_0$ the oscillation amplitude at resonance. The correct calculation of the phase noise is non-trivial, since the phase is a non-linear function of the two variables $x(t)$ and $y(t)$, which is non-regular at the origin and thus the common rules for noise/error propagation have to be applied with care. The correct calculation based on statistical mechanics is presented in appendix B. Here we will assume that a finite oscillation is applied to the cantilever in order to prevent the system to be near the origin of the $\{x(t), y(t)\}$ phase space. Then, the mean phase is $\langle\varphi(t)\rangle_\tau = -\pi/2$[27] and the fluctuation of the phase is $\Delta\varphi_{th} = \sqrt{\langle\varphi^2(t)\rangle_\tau - \langle\varphi(t)\rangle_\tau^2} = \sqrt{\langle(\tan^{-1}(x(t)/y(t)))^2\rangle_\tau}$. Using the relation $\langle f^{\,2}(z_0+z)\rangle = f^2(z_0) + |f'(z_0)|^2\langle z^2\rangle$ we have, with $f(z) = \tan^{-1}(z)$, $z(t) = x(t)/y(t)$ and $z_0 = \langle x(t)/y(t)\rangle = 0$,

$$\Delta\varphi_{th} = \sqrt{\frac{1}{1+\langle x(t)/y(t)\rangle_\tau^2}\left\langle\left(\frac{x(t)}{y(t)}\right)^2\right\rangle_\tau} = \sqrt{\frac{\langle x^2(t)\rangle_\tau}{\langle y^2(t)\rangle_\tau}} \tag{12}$$

And finally, with $\langle y^2(t)\rangle_\tau = (a_{os}^2 + a_{th}^2/2)$ and relation 10 we find for the phase noise measured around a center frequency ν_c with a bandwidth $bw = 1/\tau$:

$$\Delta\varphi_{th} = \sqrt{\frac{\Delta a_{th}^2(\nu_c, bw)/2}{a_{os}^2 + \Delta a_{th}^2(\nu_c, bw)/2}} \tag{13}$$

For large oscillation amplitude, the phase noise is therefore $\Delta a_{th}/(\sqrt{2}a_{os})$, which can be interpreted as a variation of the phase due to thermal fluctuation of magnitude $a_{th}/\sqrt{2}$ of the x-component when the y-component has an oscillation amplitude a_{os}. For very small oscillation amplitude, relation 13 would give $\Delta\varphi_{th} = 1$. However, as discussed above, at the origin of the $\{x(t), y(t)\}$ phase space the phase is mathematically not well defined, relation (12) cannot be used, and relation 13 is not accurate. On physical arguments one would expect a uniform distribution of phase, that is, a (normalized) probability distribution $p(\varphi) = 1/(2\pi)$, which has a mean deviation $\Delta\varphi = \pi/\sqrt{3}$. As shown in appendix B this is correct in the limit of vanishing oscillation (see inset of figure 3). The correct relation for the phase noise has no simple functional relation with the oscillation amplitude, therefore

we propose

$$\Delta\varphi_{th} = \sqrt{\frac{\Delta a_{th}^2\left(\nu_c, bw\right)}{2a_{os}^2 + 3\Delta a_{th}^2\left(\nu_c, bw\right)/\pi^2}} \tag{14}$$

as approximation for the correct phase fluctuation which has the correct large and low oscillation behavior. Figure 3 shows the known large oscillation behavior for phase noise, the correct relation calculated in the appendix as well as the approximations according to relations 12 and relation 14 with the correct small and large oscillation limits.

With relation 11 we finally obtain for the total frequency noise:

$$\Delta\nu_{th} = \frac{\nu_0}{2Q}\sqrt{\frac{\Delta a_{th}^2\left(\nu_c, bw\right)}{2a_{os}^2 + 3\Delta a_{th}^2\left(\nu_c, bw\right)/\pi^2}} \tag{15}$$

In order to discuss this relation, and to compare with the results known from the literature, we will consider the different approximations for large and low oscillation amplitudes, as well as for small and large bandwidth. For (very) low bandwidth, and large oscillation amplitude we obtain, using relation 9

$$\Delta\nu_{th} = \frac{\nu_0}{2Q}\sqrt{\frac{1}{\pi}\frac{kT}{ca_{ex}^2}\frac{Q}{\nu_0}}\sqrt{bw}$$

which is similar to the result reported in the literature[17, 18, 20] (relation 2). As discussed in the previous section, this (very) "low bandwidth approximation" is usually not valid. On the contrary, we believe that in most applications the bandwidth is larger than the width of the resonance curve. Then, as long as instrumental noise is negligible, the correct approximation would be a "large bandwidth" approximation where all the thermal noise is "seen" by the DSFM - detection system. In this case the corresponding (total) frequency noise is

$$\Delta\nu_{th} = \frac{\nu_0}{2Q}\sqrt{\frac{1}{3/\pi^2 + 2a_{ex}^2/a_{th}^2}} \tag{16}$$

which is $\Delta\nu_{th} \simeq (\nu_0/Q)\, a_{th}/(2\sqrt{2}a_{ex})$ for large amplitude and for $\pi/\left(2\sqrt{3}\right)\ \nu_0/Q \simeq 0.9\,\nu_0/Q$ for low amplitude. The characteristic frequency determining the thermal frequency noise is therefore the width ν_0/Q of the resonance curve, and for low oscillation amplitudes ($a_{os} \ll a_{th}$) the thermal frequency noise is essentially given by the width of the resonance curve. In particular, this implies that, as demonstrated recently for spectroscopy applications[35], DSFM is possible without external excitation of the tip-sample system. Moreover, we believe that a properly designed DFSM-electronics should be able to lock onto the thermal noise of the cantilever.

V. EXPERIMENTS

In order to confirm the validity of the relations just discussed, noise measurements have been made as a function of the bandwidth and the oscillation amplitude. A commercial SFM - system based on optical beam deflection[29] was used to measure cantilever motion and analysis of cantilever oscillation was performed either with the DSFM electronics[29] or with a digital lock-in amplifier[30]. The set-up of the SFM system and the essential features of the DSFM electronics are shown in figure 1[31]. A cantilever with a nominal force constant $c \simeq 0.4N/m$[32] was used and the tip was kept at a large ($1mm$) distance from the sample. For this kind of cantilever, relation 1 gives a total mean (rms) fluctuation of $100pm$. Figure 4 shows the the spectral noise measurement of the cantilever movement acquired with the digital locking amplifier[30]. To characterize the spectral noise density and to discriminate thermal noise against other (technical) noise sources this data is fitted to the function

$$f(\nu) = \frac{\alpha_{th}}{\sqrt{(1-(\nu/\nu_0)^2)^2 + ((\nu/\nu_0)/Q)^2}} + n^0_{tec}$$

The Lorentzian function is used to describe the thermal noise density of the cantilever, and the constant n^0_{tec} is introduced to describe any additional (technical) noise (see also [9, 36]). From the fit to the experimental data, a quality factor $Q = 100 \pm 1$, a natural frequency $\nu_0 = 79.440 \pm 0.002$kHz, a thermal noise density α_{th}=26.4±0.2 fm/$\sqrt{\text{kHz}}$ and a constant n^0_{tec}=17±2 fm/$\sqrt{\text{kHz}}$ is found.

The inset of figure 4 shows the total noise as a function of bandwidth, with the central frequency of the noise measurements at the resonance peak. In this log-log plot the square root dependence of the total noise on bandwidth for small bandwidth is clearly recognized from the slope $m = 1/2$. For high bandwidth, the total noise saturates. This saturation occurs for a bandwidth of the order of the width of the resonance curve $\Delta\nu = \nu_0/Q \simeq 0.8kHz$, in good agreement with the discussion above (relations 13 and 16) and the data obtained from the spectral noise density. The saturation of noise is only observed if other noise sources are negligible, which is clearly the case in our measurements. Therefore, as the bandwidth of noise measurement is increased only the thermal noise in the resonance peak is "seen" by the DSFM detection unit. When other noise sources are not negligible, as the bandwidth of the DSFM detection unit is increased ($bw > \nu/Q$), the detection unit will "see" this additional noise and the total noise will not saturate. Instead, it will continue

to increase with the square root dependence known from the literature[38]. If the technical noise is appreciable, a total noise well above the theoretical value $\Delta a_{th} = \sqrt{kT/c}$ for thermal noise can be experimentally observed since thermal and technical noise is measured.

Finally, figure 5 shows the noise of the frequency as a function of oscillation amplitude. Two different regimes are recognized: a constant regime for low oscillation amplitude where the total noise is independent of oscillation amplitude and a second regime where, as evidenced by the slope $m = -1$ in the $\log(noise)$ vs. $\log(a_{os})$ plot, the noise decreases with the inverse of the oscillation amplitude. The transition range of this graph corresponds to an oscillation amplitude $\sqrt{kT/c} \simeq 100pm$, in good agreement with the value for the thermal oscillation amplitude obtained from the frequency noise measurement shown in figure 4.

VI. SUMMARY

In the present work we have revised DSFM frequency detection and have analyzed how the thermal fluctuation of the cantilever is processed by a DSFM detection electronics. We find a general relation for the frequency noise as a function of a bandwidth and oscillation amplitude. This relation is correct for all possible values of parameters, while the relation known so far from the literature is only correct for a particular range. We find that for sufficiently large bandwidth -that is, small time constants of the DSFM detection electronics- essentially all the thermal noise of the cantilever is measured. In this case the width of the resonance peak is the characteristic noise of any DSFM frequency measurement for small oscillation amplitude. For larger oscillation amplitude the noise decreases linearly with the oscillation amplitude. In the large amplitude and (very) low bandwidth limit our general relation converges within a constant factor, to the relation known from the literature.

We are convinced that the results presented in this work are relevant for the precise determination of the ultimate limits of DSFM. In particular, our general relation shows that for small oscillation amplitudes the frequency noise does not diverge, but rather converges towards a finite value. Therefore, small oscillation DSFM might be much more competitive than considered up to now. DSFM without external oscillation, that is, driven by thermal noise, might be possible not only for the measurement of tip-sample interaction, but also for imaging applications. Since many high precision measurements SFM measurements -in particular in the field of Electrostatic and Magnetic Force Microscopy- are ultimately based

on frequency measurements we believe that the present work will also improve understanding and optimization of these related SFM techniques and shed light on the ultimate limit of Scanning Force Microscopy in different important applications.

VII. ACKNOWLEDGMENTS

The authors acknowledge stimulating discussions with A. Urbina, J. Gómez, L. Colchero and A. Gil. The authors also thank Atomic Force F&E GmbH, and in particular Mr. Ludger Weisser, for supplying the cantilevers used. This work was supported by the Spanish Ministry of Science and Technology through the projects NAN2004-09183-C10-3 and MAT2006-12970-C02-01 as well as by the "Comunidad Autónoma de la Región de Murcia" through the proyect "Células solares orgánicas: de la estructura molecular y nanométrica a dispositivos operativos macroscópicos".

VIII. APPENDICES

A. Appendix A

In the harmonic approximation, the fundamental equation describing the dynamics of a SFM-system is that of the forced harmonic oscillator, $m\ \ddot{a}(t) + \gamma\ \dot{a}(t)\ +\ c\ a(t)\ = F(t)$, where c is the force constant of the system, m its (effective) mass, γ the constant describing the damping in the system and $F(t)$ the external force driving the oscillator. With the definitions $\omega_0 = (c/m)^{1/2}$, $Q^{-1} = \gamma/(m\omega_0) = \omega_0\gamma/c$, and assuming a harmonic driving force $F(t) = m\ a_0\omega_0^2 \cos(\omega t) = m\ a_0\omega_0^2\, \mathrm{Re}(e^{i\omega t})$, where a_0 is a displacement determined by a static force ($a_0 = F_0/c$), this equation is transformed into

$$\ddot{a}(t) + (\omega_0/Q)\ \dot{a}(t)\ +\ \omega_0^2 a(t)\ = a_0\omega_0^2 \cos(\omega t)$$

Note that, in order to avoid recurrent 2π factors the angular frequency $\omega = 2\pi\nu$ will be used here instead of the frequency ν as in the main text. For the steady state motion this equation can be solved algebraically with the classical ansatz $a(t) = \mathrm{Re}\left\{A(\omega)e^{i\omega t}\right\}$:

$$\mathrm{Re}\left\{-\omega^2 A(\omega)\ e^{i\omega t} + (\omega_0/Q)\ i\omega A(\omega)\ e^{i\omega t} + \omega_0^2\ A(\omega)\ e^{i\omega t}\right\} = \mathrm{Re}\left\{a_0\omega_0^2 e^{i\omega t}\right\}$$

from which the complex amplitude $A(\omega)$ is determined as

$$A(\omega) = \frac{a_0}{1 - (\omega/\omega_0)^2 + i(\omega/\omega_0)/Q} \tag{17}$$

A dimensionless (but complex) mechanical gain

$$G(\omega) = \frac{1}{1 - (\omega/\omega_0)^2 + i(\omega/\omega_0)/Q} \tag{18}$$

can be defined so that $A(\omega) = a_0 G(\omega)$. For the discussion that will follow, it is more convenient to describe the complex amplitude $A(\omega)$ in Cartesian coordinates:

$$X(\omega) = a_0 \frac{1 - (\omega/\omega_0)^2}{(1 - (\omega/\omega_0)^2)^2 + ((\omega/\omega_0)/Q)^2} \tag{19}$$

$$Y(\omega) = a_0 \frac{(\omega/\omega_0)/Q}{(1 - (\omega/\omega_0)^2)^2 + ((\omega/\omega_0)/Q)^2} \tag{20}$$

where $X(\omega)$ and $Y(\omega)$ are the in-phase and out of phase components of the oscillation. Then the complex amplitude is $A(\omega) = X(\omega) - iY(\omega)$ and the time response to the excitation $a_0\omega_0^2 \cos(\omega t)$ is $a(t) = X(\omega)\cos(\omega t) + Y(\omega)\sin(\omega t) = |A(\omega)| \cos(\omega t + \varphi(\omega))$ with a phase $\varphi(\omega)$. This phase describes the delay between the excitation and the response,

$$\varphi(\omega) = -\tan^{-1}\left(\frac{Y(\omega)}{X(\omega)}\right) = -\pi/2 + \tan^{-1}\left(\frac{X(\omega)}{Y(\omega)}\right) \tag{21}$$

As described in the main text, to experimentally determine state of a harmonic oscillator, the measured deflection $a(t)$ is multiplied with two reference signals $\cos(\omega_r t)$ and $\sin(\omega_r t)$ to obtain two quadrature signals

$$x_q(t) = a(t)\cos(\omega_r t) = \frac{X(\omega)}{2}(\cos(\omega_\Delta t) + \cos(\omega_\Sigma t)) + \frac{Y(\omega}{2}(\sin(\omega_\Delta t) + \sin(\omega_\Sigma t))$$

$$y_q(t) = a(t)\sin(\omega_r t) = \frac{X(\omega)}{2}(-\sin(\omega_\Delta t) + \sin(\omega_\Sigma t)) + \frac{Y(\omega)}{2}(\cos(\omega_\Delta t) - \cos(\omega_\Sigma t))$$

with $\omega_\Delta = \omega - \omega_r$ and $\omega_\Sigma = \omega + \omega_r$. With the definitions

$$\mathbf{M}_\Delta(t) = \frac{1}{2}\begin{pmatrix} \cos(\omega_\Delta t) & \sin(\omega_\Delta t) \\ -\sin(\omega_\Delta t) & \cos(\omega_\Delta t) \end{pmatrix} \text{ and } \mathbf{M}_\Sigma(t) = \frac{1}{2}\begin{pmatrix} \cos(\omega_\Sigma t) & \sin(\omega_\Sigma t) \\ \sin(\omega_\Sigma t) & -\cos(\omega_\Sigma t) \end{pmatrix}$$

the output of the two multiplication stages can be written in matrix notation as $\{x_q(t), y_q(t)\} = (\mathbf{M}_\Delta(t) + \mathbf{M}_\Sigma(t))\{X(\omega), Y(\omega)\}$. The corresponding time evolution can thus be decomposed into one vector rotating clockwise with the frequency ω_Δ and another one rotating counter-clockwise with the frequency ω_Σ. After the multiplication stage the

two quadrature signals $x_q(t)$ and $y_q(t)$ are low-pass filtered. For a simple first order low pass the corresponding time domain signals are

$$\begin{aligned}\langle x_q(t)\rangle_\tau &\equiv \frac{1}{\tau}\int_{-\infty}^{0} d\xi\ x_q(t-\xi)\ e^{\xi/\tau} \qquad (22)\\ &= \frac{X(\omega)}{2}\frac{\cos(\omega_\Delta t)-\omega_\Delta\ \tau\ \sin(\omega_\Delta\ t)}{(1+\omega_\Delta^2\tau^2)}+\frac{Y(\omega)}{2}\frac{\sin(\omega_\Delta t)+\omega_\Delta\ \tau\ \cos(\omega_\Delta\ t)}{(1+\omega_\Delta^2\tau^2)}\\ &+\frac{X(\omega)}{2}\frac{\cos(\omega_\Sigma t)-\omega_\Sigma\ \tau\ \sin(\omega_\Sigma\ t)}{(1+\omega_\Sigma^2\tau^2)}+\frac{Y(\omega)}{2}\frac{\sin(\omega_\Sigma t)+\omega_\Sigma\ \tau\ \cos(\omega_\Sigma\ t)}{(1+\omega_\Sigma^2\tau^2)}\\ \langle y_q(t)\rangle_\tau &\equiv \frac{1}{\tau}\int_{-\infty}^{0} d\xi\ y_q(t-\xi)\ e^{\xi/\tau} \qquad (23)\\ &= \frac{X(\omega)}{2}\frac{-\sin(\omega_\Delta t)-\omega_\Delta\tau\cos(\omega_\Delta\ t)}{(1+\omega_\Delta^2\tau^2)}+\frac{Y(\omega)}{2}\frac{\cos(\omega_\Delta t)-\omega_\Delta\ \tau\ \sin(\omega_\Delta\ t)}{(1+\omega_\Delta^2\tau^2)}\\ &+\frac{X(\omega)}{2}\frac{\sin(\omega_\Sigma t)+\omega_\Sigma\ \tau\ \cos(\omega_\Sigma\ t)}{(1+\omega_\Sigma^2\tau^2)}+\frac{Y(\omega)}{2}\frac{-\cos(\omega_\Sigma t)+\omega_\Sigma\ \tau\ \sin(\omega_\Sigma\ t)}{(1+\omega_\Sigma^2\tau^2)} \qquad (24)\end{aligned}$$

Again, two matrices

$$\mathbf{M}\tau_\Delta(t)=\frac{1}{2(1+\tau^2\omega_\Delta^2)}\begin{pmatrix}\cos(\omega_\Delta t)-\omega_\Delta\tau\sin(\omega_\Delta t) & \sin(\omega_\Delta t)+\omega_\Delta\tau\cos(\omega_\Delta t)\\ -\sin(\omega_\Delta t)-\omega_\Delta\tau\cos(\omega_\Delta t) & \cos(\omega_\Delta t)-\omega_\Delta\tau\sin(\omega_\Delta t)\end{pmatrix} \qquad (25)$$

$$\mathbf{M}\tau_\Sigma(t)=\frac{1}{2(1+\tau^2\omega_\Sigma^2)}\begin{pmatrix}\cos(\omega_\Sigma t)-\omega_\Sigma\tau\sin(\omega_\Sigma t) & \sin(\omega_\Sigma t)+\omega_\Sigma\tau\cos(\omega_\Sigma t)\\ \sin(\omega_\Sigma t)+\omega_\Sigma\tau\cos(\omega_\Sigma t) & -\cos(\omega_\Sigma t)+\omega_\Sigma\tau\sin(\omega_\Sigma t)\end{pmatrix} \qquad (26)$$

can be defined. The first matrix, $\mathbf{M}\tau_\Delta(t)$, corresponds to a clockwise rotation with the frequency ω_Δ and a delay angle $\varphi_\Delta = -\tan(\omega_\Delta\tau)$ while the second matrix, $\mathbf{M}\tau_\Sigma(t)$, corresponds to a counter-clockwise rotation with the frequency ω_Σ and a delay angle $\varphi_\Sigma = +\tan(\omega_\Sigma\tau)$.

B. Appendix B

For the calculation of the variation of the phase, we will assume that the variables $x(t)$ and $y(t)$ are Gaussian variables. At resonance, as discussed above $\langle x(t)\rangle_\tau = 0$ and $\langle y(t)\rangle_\tau = Qa_{exc} = a_{os}$, therefore their probability distributions are described by

$$p_x(x)=\sqrt{\frac{1}{\pi a_{th}^2}}e^{-(x/a_{th})^2}$$

$$p_y(y)=\sqrt{\frac{1}{\pi a_{th}^2}}e^{-((y-a_{os})/a_{th})^2}$$

These distributions are normalized and have the standart deviation $\Delta x = \Delta y = a_{th}/\sqrt{2} = \sqrt{kT/(2c)}$. To calculate the distribution of the phase, first its probability function has to be calculated according to the general relation (see, for example, [39]),

$$p_\varphi(\varphi) = \iint dx\ dy\ p_x(x)\ p_y(y)\ \delta(\varphi - \tan^{-1}(x/y))$$

which in our case leads to

$$\begin{aligned}
&= \frac{1}{\pi a_{th}^2}\iint dx\ dy\ e^{-(x/a_{th})^2} e^{-((y-a_{os})/a_{th})^2}\ \delta(\varphi - \tan^{-1}(x/y)) \\
&= \frac{1}{\pi a_{th}^2}\iint d\vartheta r dr\ e^{-(r\sin(\vartheta)/a_{th})^2} e^{-((r\cos(\vartheta)-a_{os})/a_{th})^2}\ \delta(\varphi - \tan^{-1}(r\sin(\vartheta)/r\cos(\vartheta))) \\
&= \frac{1}{\pi a_{th}^2}\iint d\vartheta r dr\ e^{-(r^2-2r\cos(\vartheta)a_{os}+a_{os}^2)/a_{th}^2)}\ \delta(\varphi - \vartheta) = \frac{1}{\pi a_{th}^2} e^{-a_{os}^2\sin^2(\varphi)/a_{th}} \int_0^\infty r dr\ e^{-(r-\cos(\varphi)a_{os})^2/a_{th}^2)} \\
&= \frac{1}{\pi a_{th}^2} e^{-a_{os}^2\sin^2(\varphi)/a_{th}^2} \left(\int_0^\infty dr\ (r - \cos(\varphi)\, a_{os})\ e^{-(r-\cos(\varphi)a_{os})^2/a_{th}^2)} + \cos(\varphi)\, a_{os} \int_0^\infty dr\ e^{-(r-\cos(\varphi)a_{os})^2/a_{th}^2)} \right) \\
&= \frac{1}{\pi a_{th}^2} e^{-a_{os}^2\sin^2(\varphi)/a_{th}^2} \left(\frac{a_{th}^2}{2}\ e^{-\cos^2(\varphi)a_{os}^2/a_{th}^2)} + \cos(\varphi)\, a_{os} \frac{\sqrt{\pi}}{2} a_{th}(1 + \mathrm{Erf}[a_{os}\cos(\varphi)/a_{th}]) \right) \\
&= \frac{1}{2\pi} \left(e^{-a_{os}^2/a_{th}^2} + \sqrt{\pi}\ \frac{a_{os}}{a_{th}}\ e^{-a_{os}^2\sin^2(\varphi)/a_{th}^2} \cos(\varphi) \left(1 + \mathrm{Erf}\left[\frac{a_{os}}{a_{th}} \cos(\varphi) \right] \right) \right) \qquad (27)
\end{aligned}$$

where $\mathrm{Erf}[x] = 2/\sqrt{\pi}\int dx\ e^{-x^2}$ is the normalized Error Function ($\mathrm{Erf}[\infty] = 1$). This probability distribution is plotted in the inset of figure 3 for the range of oscillation amplitudes $a_{os}/a_{th} = 0-2$. For large oscillation amplitude $a_{os} >> a_{th}$ the first term can be neglected, in addition we can assume $\mathrm{Erf}[...] \simeq 1$, and only very small angles contribute to the probability amplitude ($\sin(\varphi) \simeq \varphi$; $\cos(\varphi) \simeq 1$) then, with $\varphi_{th} \equiv a_{th}/a_{os}$, we find

$$p_\varphi(\varphi) \simeq \frac{1}{\sqrt{\pi}\varphi_{th}} e^{-\varphi^2/\varphi_{th}^2}$$

which is a normalized Gaussian probability distribution of the angle φ with standart deviation $\Delta\varphi = \varphi_{th}/\sqrt{2} = a_{th}/(\sqrt{2}a_{os})$, in agreement with the high excitation limit of eq. 13. We note that the ratio $\varphi_{th} \equiv a_{th}/a_{os}$ can be interpreted as the fluctuation of the phase due to thermal variation $a_{th}/\sqrt{2}$ of the x-component when the y-component of the oscillation is fixed at a_{os} (for $a_{os} >> a_{th}$ thermal fluctuation of the y-component essentially gives no

contribution to phase noise). For small oscillation amplitudes the second term in 27 is small and we find, to first order in $1/\varphi_{th}$,

$$p_\varphi(\varphi) \simeq \frac{1}{2\pi}\left(1 + \frac{2\sqrt{\pi}}{\varphi_{th}}\cos(\varphi)\right)$$

The angle probability distribution therefore becomes non-Gaussian and ultimately uniform (see inset of figure 3), as is expected for vanishing oscillation amplitude. The mean value of this (normalised) angle distribution is $\overline{\varphi} = 0$, and its square deviation $(\Delta\varphi)^2 = \pi^2/3 - 2\sqrt{\pi}\varphi_{th}$. The correct phase error $\Delta\varphi\,(a_{os}/a_{th})$ calculated from the probability distribution 27 is plotted in figure 3, together with the different approximations discussed in this work.

IX. FIGURE CAPTIONS

Figure 1

Schematic description of a typical lock-in type DSFM detection unit. The signal to be analyzed by the DSFM detection is assumed to be centered around some frequency ν_0. It enters the detection unit at the input "*in*", is amplified and usually high-pass filtered (for simplicity the corresponding components are not shown) before being multiplied with two reference signals in quadrature at a frequency ν_{ref}. After this multiplication, the signal is shifted to the frequencies $\nu_0 - \nu_{ref}$ and $\nu_0 + \nu_{ref}$. The resulting signals are then low-pass filtered to remove the higher frequency component $(\nu_0 + \nu_{ref})$, resulting in two averaged signals $\langle x(t)\rangle_\tau$ and $\langle y(t)\rangle_\tau$. For sufficiently small interaction $\langle x(t)\rangle_\tau$ is proportional to the frequency shift and can be used to re-adjust the driving frequency of the VCO (or NCO) by means of an appropriate feedback loop (PI-controller). The output of the PI-controller used to adjust the excitation frequency is then proportional to the frequency shift $\delta\nu(t)$.

Figure 2

Simple approximation of the noise density (black) for a thermally excited cantilever as discussed in the main text together with the correct noise density (red). For large quality factors, most of the noise is within the main peak at the resonance frequency.

Figure 3

Main graph: Thermal noise error of the phase as a function of the (relative) oscillation amplitude a_{os}/a_{th}. The black, solid, thin line ending at $\Delta\varphi(0) = 1$ corresponds to the relation obtained from the relation known in the literature, which diverges for small oscillation

amplitude. The black, dotted line corresponds to the relation $\Delta\varphi_{th} = \sqrt{\langle(\tan^{-1}(x/y))^2\rangle}$ (12), which is not correct at the singular point $\{x, y\} = \{0, 0\}$. The red, thick, solid line shows the correct relation calculated from the probability distribution discussed in the appendix B (see inset and relation 27). Finally, the red, thin, dotted line corresponds to the approximation $\Delta\varphi_{th} = \sqrt{a_{th}^2/(2a_{os}^2 + 3a_{th}^2/\pi^2)}$ (relation 14), which has the correct low and large amplitude limits.

Inset: Probability distributions $p_\varphi(\varphi)$ for different (relative) oscillation amplitude a_{os}/a_{th}. The probability distributions have been calculated for the range of oscillation amplitudes $a_{os}/a_{th} = 0 - 2$. The probability distribution $p_\varphi(\varphi)$ for $a_{os}/a_{th} = 0$ is flat while that for $a_{os}/a_{th} = 2$ is essentially Gaussian and has the highest peak at $\varphi = 0$

Figure 4

Main graph: Spectral noise density of a 0.4N/m cantilever measured with a digital lock-in amplifier. For this noise measurement, no external excitation was applied to the cantilever and the motion of the cantilever was measured using the beam-deflection technique. The larger (red) points correspond to experimental noise data, the solid line to a fit assuming a constant offset and a Lorenz function (see main text) and the smaller (pink) points show the error between this fit and the measured data points. Inset: Log-Log plot of the total noise as a function of bandwidth for a noise measurement centered at the peak of the main noise curve. For small bandwidth, the frequency noise shows the typical $1/a_{os}$ behavior (slope -1 in the Log-Log plot). However, for high bandwidth ($bw > \nu_0/Q$, with Q quality factor) the total noise saturates.

Figure 5

Frequency noise of the DSFM detection electronics measured as a function of oscillation amplitude for two different bandwidths (50 Hz and 100 Hz). For this measurement, the same cantilever as that used for the previous experiment was utilized (force constant of 0.4N/m). The cantilever was excited by the DSFM electronics with the phase-locked loop enabled, and the frequency output $\delta\nu(t)$ was fed into a digital lock-in amplifier in order to determine the total noise of the frequency measurement of the DSFM detection unit. For small oscillation amplitude of the cantilever ($a_{osci} < a_{th}$, see main text), the frequency noise is independent of oscillation amplitude. For large amplitude the noise decreases linearly (slope 1 in the

$log - log$ plot).

---

[1] G. Binnig, C.F. Quate and Ch.Gerber, *Phys. Rev. Letter* **56**, 930-933 (1986).

[2] Y. Martin, C.C. Williams, H.K. Wickramasinghe, *J. Appl. Phys.* **61**, 4723 (1987).

[3] F. Ohnesorge and G. Binnig, *Science* **260** 1451 (1993).

[4] F.J. Giessibl *Science* **267**, 68-71 (1995).

[5] Y. Sugawara, M. Otha, H. Ueyama and S. Morita *Science* **270**, 1646 (1995).

[6] Y. Sugimoto, P. Pou P, M. Abe M, P. Jelinek, R Perez R, S Morita, O. Custance, *Nature* **446**, 64-68 (2007).

[7] S. Hembacher, F.J. Giessibl and J. Mannhart, *Science* **305**, 380-383 (2004).

[8] U. Dürig, J.K. Gimzewski and D.W. Pohl, *Phys. Rev. Letters*, **57** (19), 2403-2406 (1986).

[9] J. L. Hutter and J. Bechhoefer *Rev. Sci. Instruments* **64** (7) (1993).

[10] H. J. Butt and M. Jaschke, *Nanotechnology* **6** (1), 1-7 (1995).

[11] J. Colchero, Reibungsmikroskopie (Scanning Force and Friction Microscopy), Reihe Konstanzer Dissertationen, Hartung-Gore Verlag, Konstanz, ISBN 3-89191-725-2, 1993.

[12] M. G. L. Gustafsson and J Clerke, *J. Appl. Phys.* **76** 1 (1994).

[13] J. Colchero, Procedures in Scanning Probe Microscopy, Chaper 1.3.3.1 "Bouncing Beam Deflection", 122-128, Editors: A. Engel, J. Frommer, H. Gaub, A. Gewirth, R. Guckenberger, M-H. Hara, W. Heckel and B. Parkinson, John Wiley & Sons (1998).

[14] F.J. Giessibl, H. Bielefeldt, S. Hembacher and J. Mannhard, *Applied Surface Science* **140**, 352-357 (1999).

[15] S. Hembacher, F.J. Giessibl and J. Mannhard, *Applied Surface Science* **188**, 445-449 (2002).

[16] D. Rugar, R. Budaklan, H.J. Mamin and B.W. Chul, *Nature* **470**, 329-332 (2004).

[17] T.R. Albrecht, P. Grütter, D. Horne and D. Rugar, *J. Appl. Phys.* **69** (2), 668-673 (1991).

[18] U. Dürig, O. Züger and A. Stalder, *J. Appl. Phys.*, **72**, 1778-1798 (1992).

[19] R. Garcia and R. Pérez, *Surface Science Reports* **47** 197-301 (2002).

[20] F.J. Giessibl 1995, *Rev. Mod. Physics* **75** 949-983 (2003).

[21] U. Dürig, H.R. Steinauer and N. Blanc, *J. Appl. Phys.* **82** (8) 3641-3651 (1997).

[22] D.P.E. Smith, *Rev. Sci. Instuments* **66** (5), 3191-3195 (1995).

[23] We note that the different use of frequency ν and angular frequency ω may lead to considerable

confusion. In the present work we will try to define all quantities in such a way that their functional appearance is the same. independently of whether frequency or angular frequency is used. Mostly frequency will be used, and the use of angular frequency will be limited to terms like $\sin(\omega t)$ and $\cos(\omega t)$ where the factor 2π -as in $\sin(2\pi\nu t)$-would be unnecessary bulky. In particular spectral densities -as in 6- are referred to frequency and not to angular frequency.

[24] S. Rast, C. Wattinger, U. Gysin and E.Meyer, *Nanotechnology* **11** 169-172 (2000).

[25] S. Rast, U. Gysin, P. Ruff, C. Gerber, E. Meyer and D.W. Lee, *Nanotechnology* **17** (7) S189-S194 (2006).

[26] D. Rugar and P Gruetter, *Physical Review Letters* **67** (22), 699-902 (1991).

[27] This may seem evident since we assume that the system is at resonance. Mathematically, however, it is important that a finite oscillation amplitude "defines" the mean angle: $\langle\varphi(t)\rangle_\tau \simeq -\pi/2 + \langle x(t)/y(t)\rangle_\tau \simeq -\pi/2 + \langle x(t)\rangle_\tau / \langle y(t)\rangle_\tau = -\pi/2 + 0/(Qa_{exc}) = -\pi/2$, for $a_{exc} \neq 0$, while for $a_{exc} = 0$ this relation -and thus the mean angle- is undefined.

[28] E. Palacios-Lidón, B. Pérez-García, J. Colchero, "Enhancing Dynamic Scanning Force Microscopy in air: As close as possible", *Nanotechnology* 20, 085707-1–085707-7 (2009).

[29] Nanotec Electronica, E-28760 Tres Cantos, www.nanotec.es.

[30] Stanford Research Instruments model:dual channel 102kHz digital lock-in amplifier.

[31] Note, however, that an optional oscillation amplitude gain control, usually used in DSFM to measure dissipation, is not included in figure 1. For the frequency noise measurements to be discussed here the gain control of the DSFM electronics was disabled and is thus not relevant in the present context.

[32] Olympus Optical Co. LDT, OMCL-RC series, short, hard cantilever (length $100\mu m$, width $20\mu m$), nominal force constant: $0.4\ N/m$. For more information see www.olympus.co.jp/probe .

[33] R. Luethi, E. Meyer, M. Bammerlin, A. Baratoff, L. Howald, C. Gerber and H.J. Guentherodt, *Surf. Rev. Lett.* **4**, 1025-1027 (1997).

[34] F.J. Giessibl, M. Herz and J. Mannhart, *PNAS* **99** (19) 12006-12010 (2002).

[35] A. Gannepalli, A. Sebastian, J. Cleveland and M. Salapaca, *Applied Physics Letters* **87**, 111901-1 - 111901-3 (2005).

[36] J. Colchero, Procedures in Scanning Probe Microscopy, Chapter 1.3.3.12 "Force Calibration",

pp. 133-138, Editors:.A. Engel, J. Frommer, H. Gaub, A. Gewirth, R. Guckenberger, M-H. Hara, W. Heckel and B. Parkinson, John Wiley & Sons (1998).

[37] H.J. Butt, B. Capella and M. Kappl, *Surface Science Reports* **59**, 1-152 (2005).

[38] More precisely: only for constant noise density the increase of total noise with will have a square root dependence. Note that if the noise density has essentially two ranges, one where the thermal noise is dominant and another one where a (constant) technical noise density is relevant, in the log-log plot this will give rise to two regions, both with slope 1/2 and thus parallel, but with a slight offset induced by the transition from the frequency range dominated by thermal noise to the frequency range dominated by technical noise.

[39] F. Schwabl, Statistical Mechanics, Springer Verlag, ISBN 3-540-43163-2 (2002).

X. FIGURES

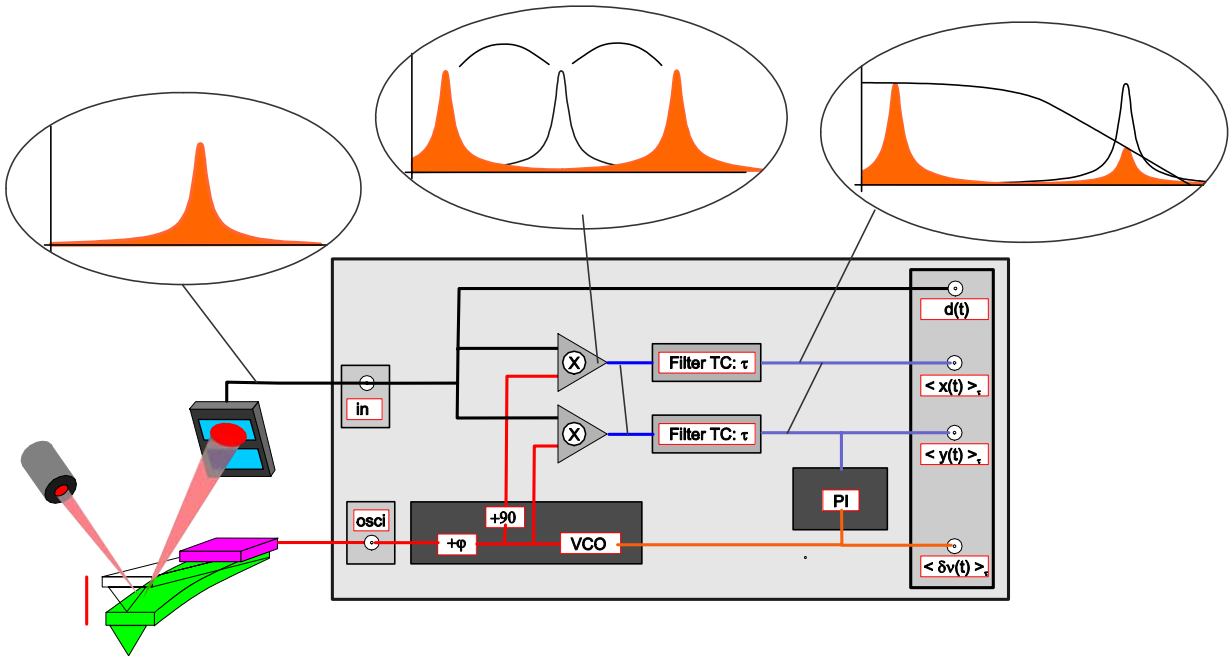

Figure 1: Schematic description of a typical lock-in type DSFM detection unit. The signal to be analyzed by the DSFM detection is assumed to be centered around some frequency ν_0. It enters the detection unit at the input "*in*", is amplified and usually high-pass filtered (for simplicity the corresponding components are not shown) before being multiplied with two reference signals in quadrature at a frequency ν_{ref}. After this multiplication, the signal is shifted to the frequencies $\nu_0 - \nu_{ref}$ and $\nu_0 + \nu_{ref}$. The resulting signals are then low-pass filtered to remove the higher frequency component $(\nu_0 + \nu_{ref})$, resulting in two averaged signals $\langle x(t)\rangle_\tau$ and $\langle y(t)\rangle_\tau$. For sufficiently small interaction $\langle x(t)\rangle_\tau$ is proportional to the frequency shift and can be used to re-adjust the driving frequency of the VCO (or NCO) by means of an appropriate feedback loop (PI-controller). The output of the PI-controller used to adjust the excitation frequency is then proportional to the frequency shift $\delta\nu(t)$.

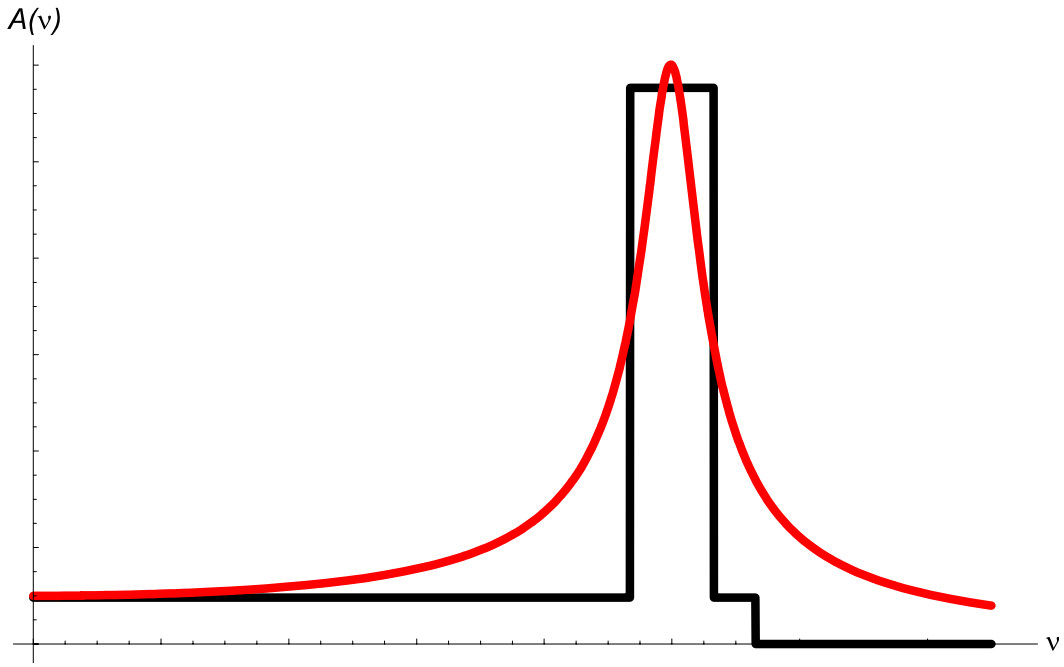

Figure 2: Simple approximation of the noise density (black) for a thermally excited cantilever as discussed in the main text together with the correct noise density (red). For large quality factors, most of the noise is within the main peak at the resonance frequency.

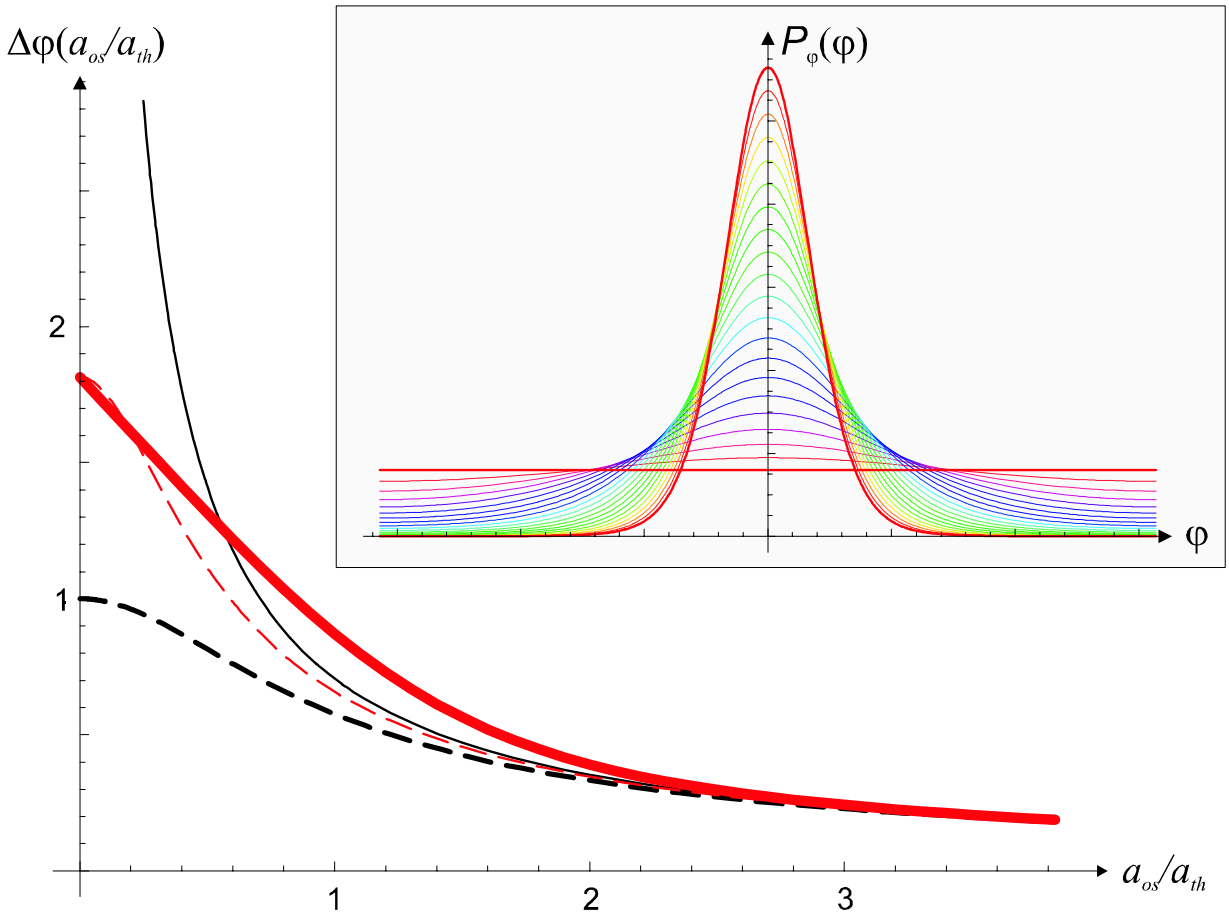

Figure 3: Main graph: Thermal noise error of the phase as a function of the (relative) oscillation amplitude a_{os}/a_{th}. The black, solid, thin line ending at $\Delta\varphi(0) = 1$ corresponds to the relation obtained from the relation known in the literature, which diverges for small oscillation amplitude. The black, dotted line corresponds to the relation $\Delta\varphi_{th} = \sqrt{\langle(\tan^{-1}(x/y))^2\rangle}$ (12), which is not correct at the singular point $\{x, y\} = \{0, 0\}$. The red, thick, solid line shows the correct relation calculated from the probability distribution discussed in the appendix B (see inset and relation 27). Finally, the red, thin, dotted line corresponds to the approximation $\Delta\varphi_{th} = \sqrt{a_{th}^2/(2a_{os}^2 + 3a_{th}^2/\pi^2)}$ (relation 14), which has the correct low and large amplitude limits.

Inset: Probability distributions $p_\varphi(\varphi)$ for different (relative) oscillation amplitude a_{os}/a_{th}. The probability distributions have been calculated for the range of oscillation amplitudes $a_{os}/a_{th} = 0 - 2$. The probability distribution $p_\varphi(\varphi)$ for $a_{os}/a_{th} = 0$ is flat while that for $a_{os}/a_{th} = 2$ is essentially Gaussian and has the highest peak at $\varphi = 0$.

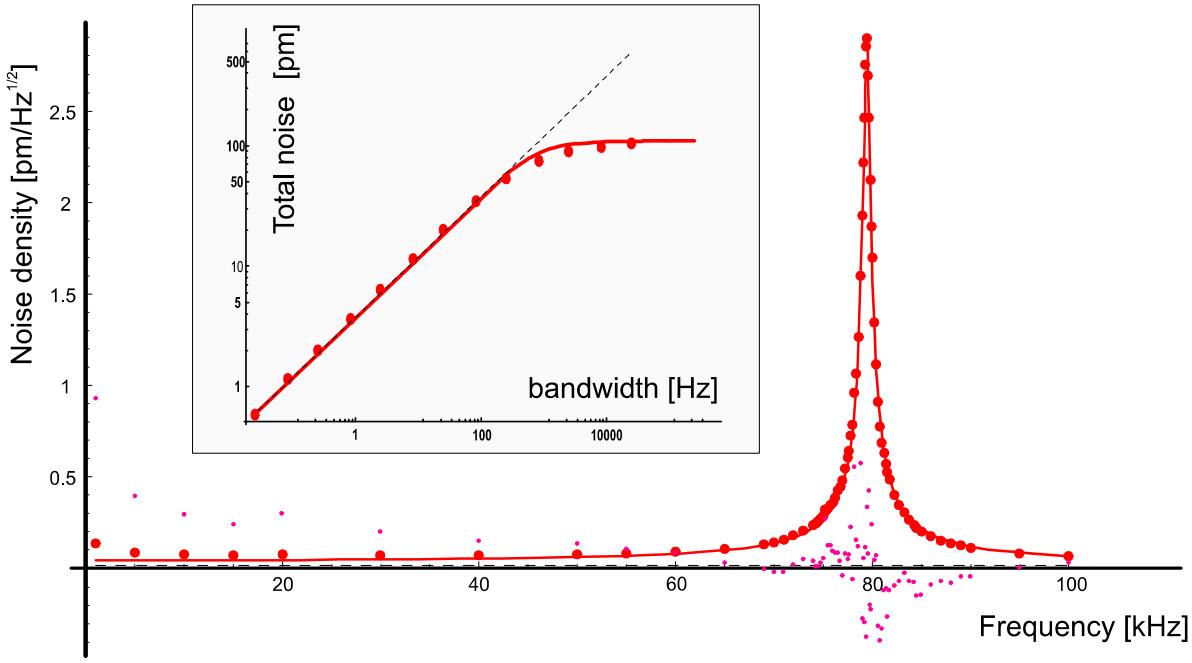

Figure 4: Main graph: Spectral noise density of a 0.4N/m cantilever measured with a digital lock-in amplifier. For this noise measurement, no external excitation was applied to the cantilever and the motion of the cantilever was measured using the beam-deflection technique. The larger (red) points correspond to experimental noise data, the solid line to a fit assuming a constant offset and a Lorenz function (see main text) and the smaller (pink) points show the error between this fit and the measured data points. Inset: Log-Log plot of the total noise as a function of bandwidth for a noise measurement centered at the peak of the main noise curve. For small bandwidth, the frequency noise shows the typical $1/a_{os}$ behavior (slope -1 in the Log-Log plot). However, for high bandwidth ($bw > \nu_0/Q$, with Q quality factor) the total noise saturates.

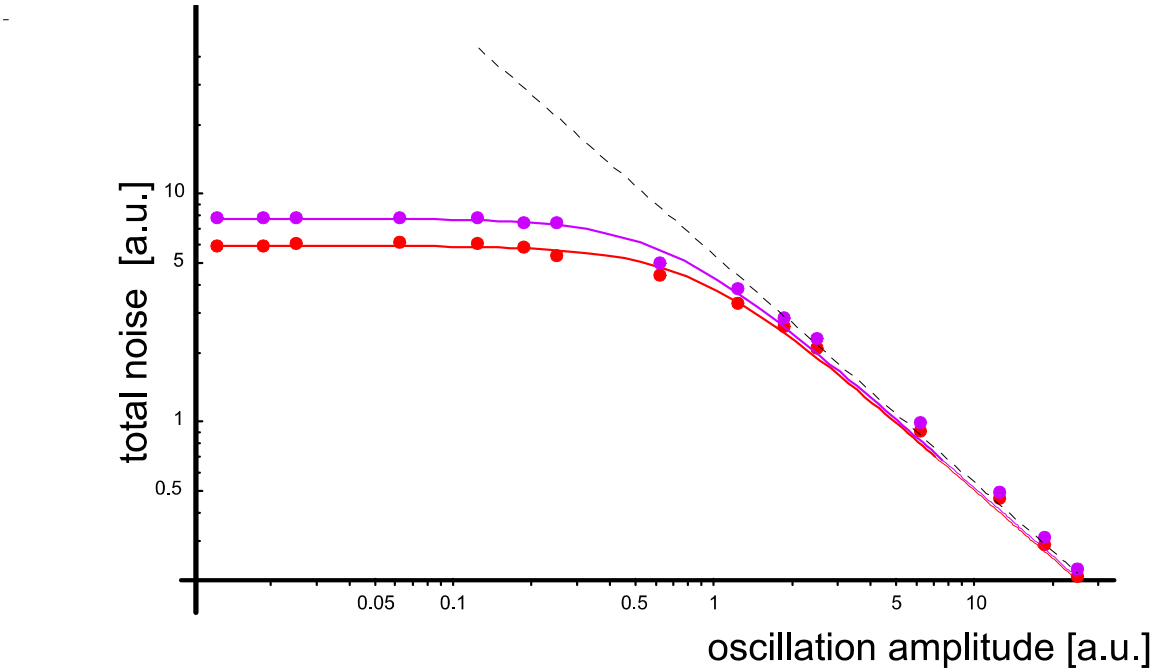

Figure 5: Frequency noise of the DSFM detection electronics measured as a function of oscillation amplitude for two different bandwidths (50 Hz and 100 Hz). For this measurement, the same cantilever as that used for the previous experiment was utilized (force constant of 0.4N/m). The cantilever was excited by the DSFM electronics with the phase-locked loop enabled, and the frequency output $\delta\nu(t)$ was fed into a digital lock-in amplifier in order to determine the total noise of the frequency measurement of the DSFM detection unit. For small oscillation amplitude of the cantilever ($a_{osci} < a_{th}$, see main text), the frequency noise is independent of oscillation amplitude. For large amplitude the noise decreases linearly (slope 1 in the $log - log$ plot).